Far infrared attenuated total reflection spectroscopy for investigating superlattice phonon parameters

1996 J. Phys.: Condens. Matter 8 8027

(http://iopscience.iop.org/0953-8984/8/42/021)

J. Phys.: Condens. Matter **8** (1996) 8027–8039. Printed in the UK

Far infrared attenuated total reflection spectroscopy for investigating superlattice phonon parameters

A A Hamilton†, T Dumelow‡, T J Parker† and S R P Smith†

† Department of Physics University of Essex, Wivenhoe Park, Colchester CO4 3SQ, UK
‡ Departamento de Física, Universidade Federal do Rio Grande do Norte, 59072-970 Natal RN, Brasil

Received 7 May 1996

Abstract. We report on low-temperature (77 K) far infrared attenuated total reflection (ATR) spectroscopic measurements on a short period GaAs/AlAs superlattice, and discuss the optics of the modes observed. We assess the significance of the ATR technique for determining superlattice phonon parameters. We model the results using a linear chain model that incorporates the effects of interface roughness; it appears that this model is correctly modelling the phonon response.

1. Introduction

Far infrared spectroscopic techniques have increasingly been used for investigating phonons in semiconductor superlattices in recent years [1]. In particular, this type of spectroscopy provides a useful complement to Raman spectroscopy for studying phonon confinement [2]. Far infrared spectra provide additional information over those from Raman spectroscopy in that the overall dielectric function is probed in the former but not in the latter.

The far infrared technique, mainly used to study superlattice dielectric functions, has been Fourier transform spectroscopy set up to measure sample reflectivity [2–9], often at oblique incidence. Since the overall dielectric tensor of a superlattice is uniaxial, oblique incidence measurements yield information on the out-of plane component (usually designated ε_{zz}) unobtainable from normal incidence experiments [10]. A far infrared technique complementary to reflectivity is attenuated total reflection (ATR) [11]. ATR experiments on superlattices have been reported [4, 6, 11–14], and their use in providing extra information on phonon confinement has been discussed in a number of places [8, 11, 15]. However, apart from a brief report of preliminary room temperature results for this work [11], no comparison of ATR results with a microscopic lattice dynamical model has been made.

In this paper we report low-temperature ATR experiments on a short period GaAs/AlAs superlattice, and examine the optics of the various modes observed. We demonstrate the use of these results in measuring phonon confinement parameters, and relate the measured parameters to the modified linear chain model of Samson *et al* [8, 16] which includes the effects of interface roughness.

2. Dielectric function of short period superlattices

In the long wavelength limit, the symmetry of a superlattice is uniaxial. In terms of confined phonon contributions, each principal component of the resulting dielectric tensor contains

0953-8984/96/428027+13$19.50

a series of resonances at the appropriate confined mode frequencies. Chu and Chang [17] describe this tensor using equations of the form

$$\varepsilon_{xx} = \varepsilon_{yy} = \varepsilon_{xx}^{\infty}\left[1 + \sum_{\mu} \frac{S_{T\mu}}{\omega_{T\mu}^2 - \omega^2 - \mathrm{i}\omega\gamma_{T\mu}}\right] \tag{1}$$

$$\frac{1}{\varepsilon_{zz}} = \frac{1}{\varepsilon_{zz}^{\infty}}\left[1 - \sum_{\mu} \frac{S_{L\mu}}{\omega_{L\mu}^2 - \omega^2 - \mathrm{i}\omega\gamma_{L\mu}}\right] \tag{2}$$

where $\omega_{T\mu}$ and $\omega_{L\mu}$ are the frequencies of the confined TO and LO phonons respectively, $S_{T\mu}$ and $S_{L\mu}$ are their oscillator strengths and $\gamma_{T\mu}$ and $\gamma_{L\mu}$ their damping parameters. $\varepsilon_{xx}^{\infty}$ and $\varepsilon_{zz}^{\infty}$ are the principal components of the high frequency dielectric function. The summation over μ covers all phonon modes in the phonon bands of both constituents.

In practice, the oscillator frequencies and strengths in (1) and (2) are affected by interface roughness. The linear chain model of Samson *et al* [8, 16] includes the effect of this roughness by considering an average susceptibility at each site, thus accounting for the fact that in a linear chain model each site represents a layer of atoms; if interface roughness occurs, each such layer may contain a mixture of atoms.

3. Modes observed in attenuated total reflection spectroscopy

In an ATR experiment in the Otto configuration [18] light is incident through a prism at an angle θ such that total internal reflection occurs within the prism. The sample is separated from the prism base by a small gap (usually vacuum). Taking the z axis to be normal to the sample and prism base, and the incident ray within the prism to be propagating in the xz plane, we get

$$q_x = \varepsilon_0^{1/2}\omega/c \sin\theta \tag{3}$$

where ε_0 is the dielectric constant of the prism. If layer 1 is taken to be the gap, then for θ greater than the critical angle, we get $q_x > \varepsilon_1^{1/2}\omega/c$ so that q_{z1} is imaginary within the gap. Thus an evanescent wave, decaying away from the base of the prism, exists within the gap.

In frequency regions in which bulk polaritons propagate within the sample the evanescent wave can couple to the polaritons to a greater or lesser extent, effectively 'leaking' across the gap. These polariton modes are of the same type as those excited from radiation incident from a vacuum. Of more interest are the special modes that arise from the fact that q_{z1} is imaginary in the gap. These modes are localized at a particular interface or confined within one or more layers and, to a first approximation, occur at discrete frequencies at which dips occur in the ATR spectra. A characteristic feature of any such mode is that an exponential field decay, corresponding to imaginary q_z, occurs to either side of the interface or layers at which it is localized.

The modes expected from an ATR experiment on a superlattice deposited on a substrate are described in reference [15]. Here we summarize some of the more important discrete modes that might be observed for a superlattice grown on a semi-infinite substrate. In the appendix we extend the analysis to include modes in a structure containing a number of different layer types.

3.1. Surface polaritons localized at the superlattice–vacuum interface

Surface polaritons are modes localized at a single interface, and only occur in p-polarization. Taking the vacuum as layer 1, and assuming that the exponential decays in the two media

(the vacuum and the superlattice) are unperturbed by extra interfaces, the surface polariton follows the dispersion relation

$$q_x^2 = \frac{\omega^2}{c^2}\frac{(\varepsilon_{xx} - \varepsilon_1)}{(\varepsilon_{xx}/\varepsilon_1 - \varepsilon_1/\varepsilon_{zz})} \tag{4}$$

where ε_{xx} and ε_{zz} are the principal components of the superlattice dielectric function given by (1) and (2) respectively. Note that, in calculating dispersion relations suitable for modelling frequency scan experiments, damping terms should be ignored.

It is straightforward to show that, for localization to occur, ε_1 and ε_{xx} must be of opposite sign and that $q_x^2/\varepsilon_{zz} < \omega^2/c^2$. Since we are considering layer 1 to be a vacuum, the first of these two conditions requires that ε_{xx} must be negative in sign in this instance.

The assumption that the mode frequencies will be unperturbed by extra interfaces is not, of course, valid in practice due to the presence of both the prism and of the substrate. The presence of a substrate, in particular, can have a significant effect on the mode frequencies when the superlattice is thin. At frequencies at which propagation occurs in the substrate (usually corresponding to a positive dielectric function) the modes become 'leaky', and the main observed change in the spectrum is a broadening of the surface mode dips. In frequency regions in which propagation does not occur in the substrate (usually corresponding to a negative dielectric function), an exponential decay occurs in the substrate instead. Thus in this case the mode is not strictly localized at only one interface, but over both of the interfaces bounding the superlattice. Equation (4) is therefore replaced by a three layer expression, with layer 3 corresponding to the substrate [15]:

$$\frac{\varepsilon_{xx}q_{z1} + \varepsilon_1 q_{z2}}{\varepsilon_{xx}q_{z1} - \varepsilon_1 q_{z2}}\exp(-\mathrm{i}q_{z2}d) = \frac{\varepsilon_{xx}q_{z3} - \varepsilon_3 q_{z2}}{\varepsilon_{xx}q_{z3} + \varepsilon_3 q_{z2}}\exp(\mathrm{i}q_{z2}d). \tag{5}$$

Here d is the thickness of the superlattice. Equation (5) thus represents the dispersion of a perturbed surface polariton mode.

3.2. Surface polaritons localized at the superlattice–substrate interface

This type of surface polariton is commonly referred to as an interface polariton mode, but it is characterized by an exponential decay either side of the interface, as before. Assuming that the decay is not perturbed by other interfaces, equation (4) may be used with ε_1 replaced by ε_3.

In a similar manner to the surface mode localized at the vacuum–superlattice, the mode localized at the superlattice–substrate interface mode requires that ε_3 and ε_{xx} must be of opposite sign. When the additional condition that q_x must be real is imposed, it can be shown that either ε_3 is positive and ε_{xx} negative or that ε_3 is negative and both ε_{xx} and ε_{zz} positive [15].

Localization requires that q_z must be imaginary in both the substrate and the superlattice. In the case where ε_{xx} is positive and ε_3 negative this implies that $q_x > \varepsilon_{zz}^{1/2}\omega/c$, and in the case where ε_{xx} is negative and ε_3 positive it implies that $q_x > \varepsilon_3^{1/2}\omega/c$. In the standard ATR experiment, both these conditions are harder to satisfy than the equivalent condition $q_x > \varepsilon_1^{1/2}\omega/c$ required for coupling to surface polaritons at the vacuum–superlattice interface. In practice, therefore, the number of experimentally observed surface polariton modes at the superlattice–substrate interface observed in an ATR experiment is somewhat limited.

In special cases, where either ε_{zz} or ε_3 is small and positive and the other appropriate dielectric parameters are of the right sign, ATR can excite surface modes at the superlattice–substrate interface. In practice, the only frequencies at which the appropriate dielectric

component takes on a sufficiently small positive value are those just above the LO's of the superlattice (where $\varepsilon_{zz} = 0$) or of the substrate (where $\varepsilon_3 = 0$). We concentrate here on the modes associated with the superlattice LOs, since they are the only ones observed on the superlattice system considered in this paper.

With ε_{zz} positive, ε_3 must be negative and ε_{xx} positive for the surface mode to exist. ε_{xx} must therefore be positive at the LO frequency, and we follow the convention of reference [15] of describing LO modes that satisfy this condition as L^+ modes. No surface mode exists around the L^- mode, where ε_{xx} is negative.

Modes of the above type tend to be described as Berreman modes, since they are essentially the same as the modes observed by Berreman [19] at the LO frequencies of isotropic media deposited on metallic substrates. They have the peculiar property that they extend to $q_x = 0$, so that the ATR geometry is not actually required for their observation. In fact, provided ε_3 is negative, Berreman dips (actually combined Berreman–Brewster dips [15]) occur around the L^+ frequencies when performing p-polarization oblique incidence reflectivity experiments from vacuum. This phenomenon is particularly useful in measuring L^+ frequencies.

So far we have ignored the perturbing effect of the vacuum–superlattice interface. Strictly speaking, (5) rather than (4) (with ε_1 replaced by ε_3) should therefore be used to describe the Berreman modes in ATR. However, in practice any shift of Berreman modes from the L^+ frequencies is usually too small to measure.

3.3. Guided wave polaritons

Guided wave modes are confined within the superlattice, having a real q_z within the superlattice and an imaginary q_z, corresponding to an exponential field decay, within the two bounding media. In p-polarization, therefore, (5) describes the dispersion of the guided wave modes; the only difference between p-polarized guided wave modes and perturbed surface modes is that q_{z2} is real in the former and imaginary in the latter. In fact, a small change in one of the parameters in (5) (for instance, the superlattice thickness) can effectively change the nature of a mode from one type to the other, as well as changing its frequency [15]. Moreover, the appearance of the spectra is not qualitatively different.

An important aspect of guided wave polaritons is that they occur in s- as well as p-polarization. The s-polarization dispersion equation is [15]

$$\frac{q_{z1} + q_{z2}}{q_{z1} - q_{z2}} \exp(-\mathrm{i}q_{z2}d) = \frac{q_{z3} - q_{z2}}{q_{z3} + q_{z2}} \exp(\mathrm{i}q_{z2}d). \tag{6}$$

For a practical ATR experiment, q_{z3} is imaginary only where ε_3 is negative (or very small), and guided wave modes only appear within frequency intervals within which this is satisfied.

All the above description refers to a superlattice deposited on a substrate. It should be noted, however, that additional layers, such as buffer or capping layers, are often present in superlattice structures. The samples used for our present experimental investigations, for instance, have a 0.1 μm top capping layer between the superlattice itself and the vacuum. It is therefore useful to generalize equations (5) and (6) for these more complex situations. In practice, transfer matrix methods may be used to calculate dispersion curves exactly for a system containing any number of layers, as described in the appendix. The modes so described are localized within the designated structure, with an upward exponential decay in the top layer (usually vacuum) and a downward exponential decay in the bottom layer (usually the substrate). These modes may be perturbed surface modes, guided waves, or a mixture of the two depending upon whether q_z is real or imaginary in the various layers. Note, however, that the modes modelled in this way are completely localized, so the prism

is assumed to have no effect. Reflectivity calculations using multilayer optics, in contrast, include the effects of all layers including the prism.

4. Experimental details

The sample used for this investigation was the $(GaAs)_4/(AlAs)_4$ superlattice described in reference [8]. The subscript 4 refers to the number of lattice units in each superlattice layer. The overall structure consisted of 1 μm of superlattice bounded by 0.1 μm of GaAs cladding and deposited on a GaAs substrate. It was grown by molecular beam epitaxy, at Philips Research Laboratories, Redhill, with the substrate maintained at 630 °C.

The ATR experiments were performed using a silicon prism cut to give an incident angle of 20°, i.e. slightly larger that the critical angle for total internal reflection of 17.04°. The sample was held away from the base of the prism by strips of copper foil near the edge of the sample. This assembly was mounted on a 77 K cryostat and placed in the output stage of a far infrared Michelson interferometer [11]. The experiments were performed at a resolution of 0.5 cm^{-1} using a Golay detector, in front of which was placed a polarizer set up to give p-polarization.

5. Results and discussion

The experimental ATR spectra in the GaAs region are shown in figure 1. The two plots show the results with two different thicknesses of copper foil spacer representing two different ATR gaps. Also shown are theoretical spectra modelled using a superlattice dielectric tensor of the form given in equations (1) and (2). All the parameters were obtained from the linear chain model described in [8]; this model takes account of roughness at the superlattice interfaces, which in this case corresponds to an interface 'error function width' [8] of 1.4 lattice units. The vacuum gap in each case was taken to be the thickness of the copper foil spacer. It can be seen that the experimental and calculated frequencies of all the features are in good agreement. The level of the reflectivity agrees less well between experiment and theory; this is fairly common in ATR spectra of this type, and is probably due to experimental variations in the vacuum gap (due to roughness) and incident angle (due to focusing the beam).

In order to discuss the features in more detail we now consider the dispersion curves $q_x(\omega)$ of the various modes. These curves are shown in figure 2. In all cases the transfer matrix method outlined in the appendix has been used to calculate the mode frequencies. Since we are using these curves to model a frequency scan, they have been modelled using dielectric functions with damping ignored. In the case of the modes marked 4–6 in the figure, the system has been modelled as a 4 layer structure with a semi-infinite substrate. The fields in the vacuum and substrate layers thus decay exponentially. The modes marked 1–3, however, occur below the TO frequency of the substrate, so propagation within the substrate occurs. In the absence of a capping layer the relevant modes would thus be leaky surface polaritons at the superlattice–vacuum interface, and their frequencies would essentially follow equation (4), although they would be broadened by leakage into the substrate. With the capping layer present, however, they are more correctly described as leaky guided waves within the capping layer. We have therefore modelled their dispersion curves in figure 2 by assuming a three-layer structure, the bottom layer being the superlattice. We have thus ignored the substrate in modelling these curves. For leaky modes of this type

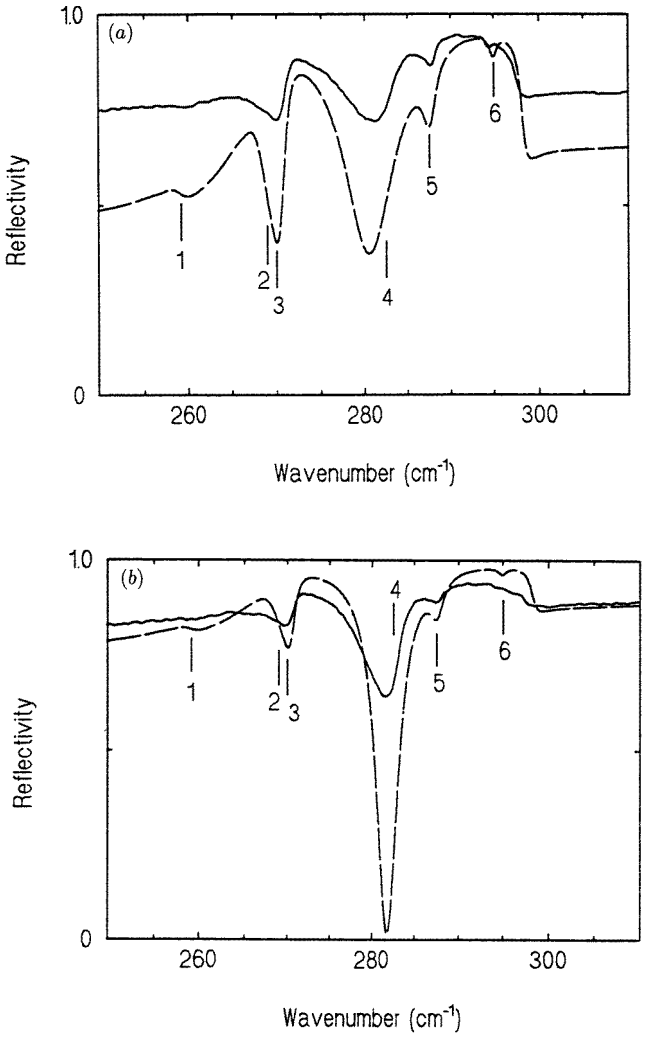

Figure 1. Experimental (solid lines) and theoretical (dashed lines) p-polarized ATR spectra, in the GaAs region, of the sample described in the text. The spectra were obtained with nominal vacuum gaps (spacer thicknesses) of (a) 7 μm and (b) 12 μm, and these values were also used for the modelled curves. The vertical lines represent the mode frequencies as determined from the dispersion curves illustrated in figure 2.

it is reasonable to do this since the main effect of the substrate on these modes will be to broaden the corresponding dips in the ATR spectrum, not to shift their frequencies.

Profiles of the H_y fields calculated for selected modes are shown in figure 3 for a 12 μm gap. In order to clarify the mode types, we have not included damping in the calculation of these profiles. Modes 1, 2 and 3 are all basically of the same type, i.e. a leaky guided wave within the capping layer, as described above. In practice, however, modes 2 and 3 cannot be resolved in the spectra. It is clear from the field profile for mode 1 in figure 3(a) that propagation into the substrate is occurring. Mode 4 is a guided wave, perturbed by the capping layer, in the superlattice, as shown in figure 3(b). Mode 5 is a Berreman mode,

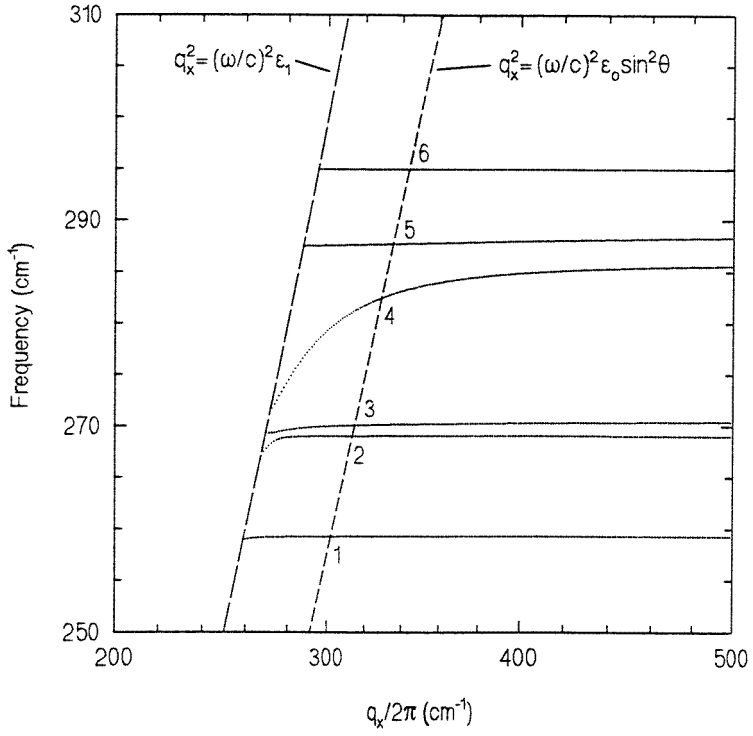

Figure 2. Dispersion curves for the surface and guided wave modes of the sample in contact with a semi-infinite vacuum.

i.e. an interface mode at the superlattice–substrate boundary. Figure 3(c) shows this mode to be very strongly localized. Its frequency is about 0.2 cm^{-1} above that of the strong L^+ mode LO_1 (the index 1 is used to indicate that the phonon mode is a fundamental with approximately 1 half-wavelength confined within each GaAs layer), although this shift is too small to discern from experimental data. Mode 6 only appears when there is a capping layer. Its frequency is just below the bulk LO frequency of the capping layer itself (and of the substrate) and it may be thought of as a surface mode on the capping layer, highly perturbed by the overall structure.

We now use the above data to examine the significance of ATR for determining phonon oscillator strengths. The use of far infrared techniques for obtaining the various parameters in (1) and (2) has been discussed theoretically in [15]. Thus, mode frequencies may be obtained by reflectivity and/or Raman. Oscillator strengths, on the other hand, are harder to measure. One method of measuring TO oscillator strengths is to use the frequency of interference features observed in s-polarization reflectivity. ATR, however, provides an alternative, and in many ways preferable, method of measuring these strengths. In the remainder of this paper we discuss the value of the observed ATR modes in determining oscillator strengths.

An important qualitative difference between the bulk or interference modes seen in reflectivity and the surface or guided wave modes observed in ATR is that the ATR modes occur at discrete frequencies that can be fairly accurately measured. In general, these

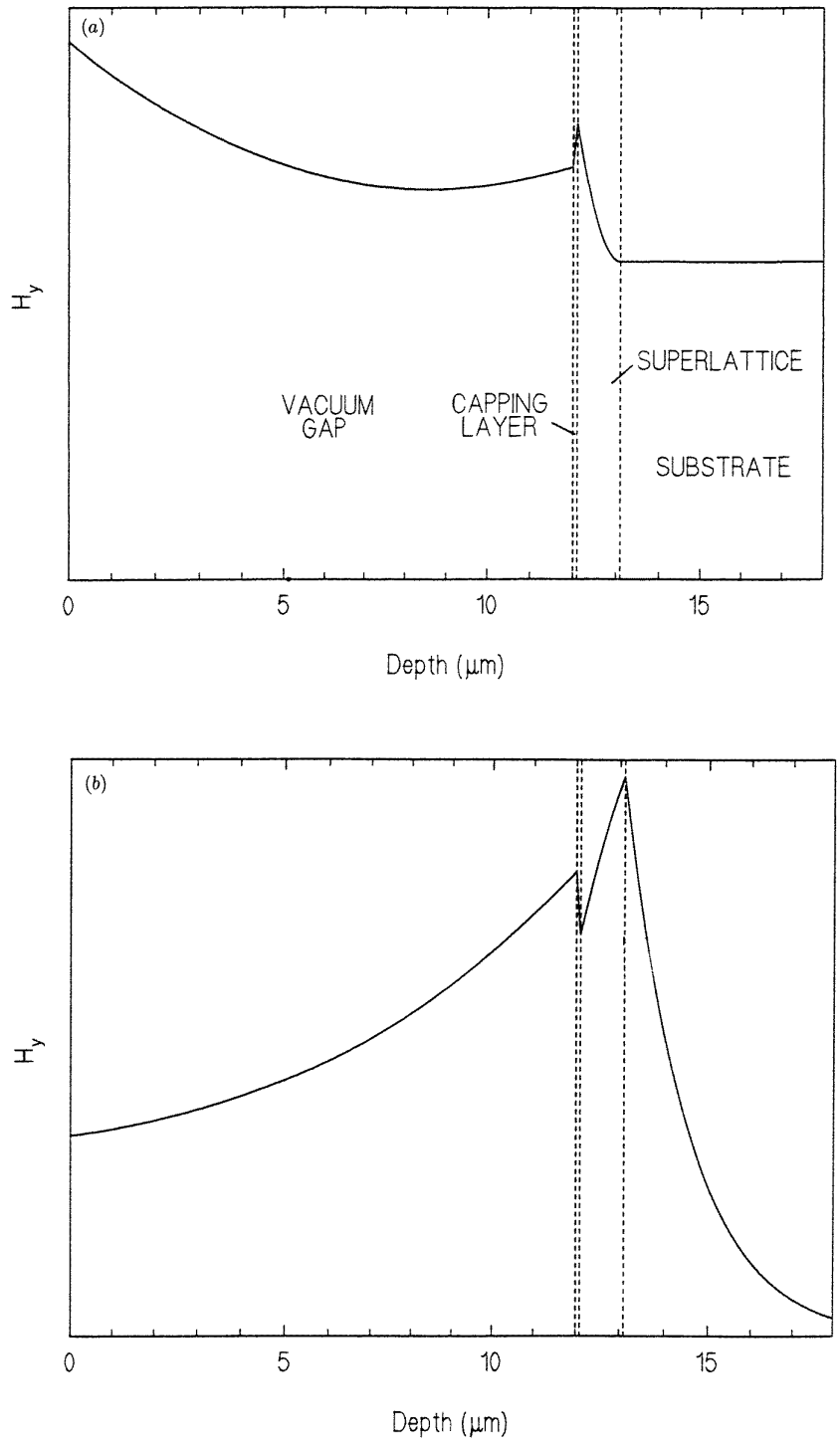

Figure 3. Magnetic field profiles H_y of some of the modes seen in figures 1 and 2: (a) mode 1, (b) mode 4, and (c) mode 5. All distances are measured from the base of the prism.

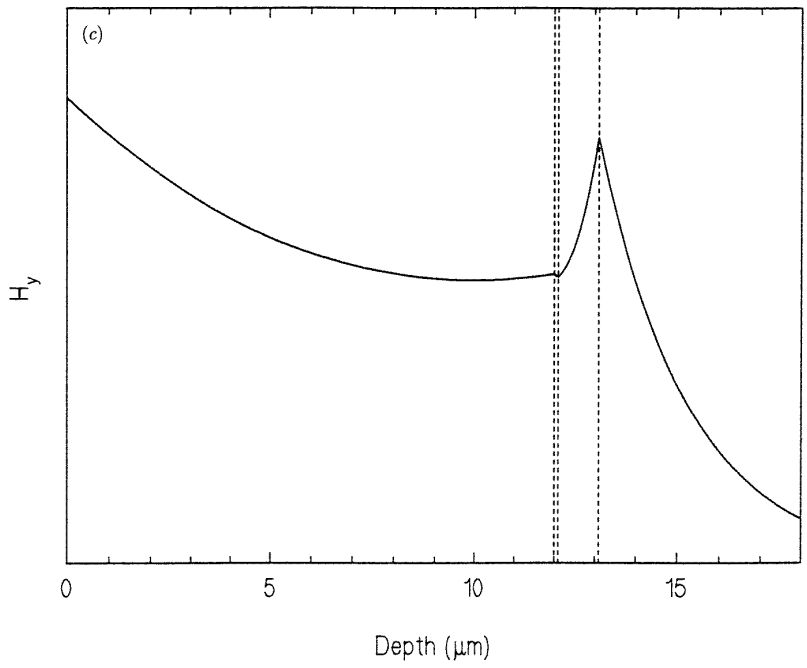

Figure 3. (Continued)

mode frequencies depend on the overall dielectric functions, so that the frequencies of the observed spectral dips depend crucially on oscillator strengths as well as on phonon frequencies. We illustrate this in figure 4. In figure 4(a) we show the variation of the various mode frequencies, calculated in the same way as for the dispersion curves, as the oscillator strength of the TO_1 mode is varied; all other parameters are those given by the linear chain model. Figure 4(b) shows the effect of varying the LO_1 oscillator strength whilst keeping the TO_1 oscillator strength fixed at the value given by the model. One can see that the frequency of mode 4 is highly sensitive to the value of the TO_1 oscillator strength, but not very sensitive to the value of the LO_1 oscillator strength. Thus it should be possible to measure TO oscillator strengths using ATR, but not to measure LO oscillator strengths with any degree of confidence.

Two reservations should be made regarding the use of ATR for measuring TO oscillator strengths. Firstly, we have considered only the strength of the fundamental TO mode (TO_1) in the GaAs region. This mode has both the greatest strength and the highest frequency of the modes in the GaAs region. The strengths of the other modes, which are both lower in frequency and weaker, have relatively little effect on the guided or surface mode frequencies. Secondly, derivation of guided or surface mode frequencies from figures 2 or 4 does not necessarily yield accurate estimates of the frequencies of the dips in the ATR spectrum. The linear chain model with interface roughness incorporated as described above yields a TO_1 oscillator strength of 6170 cm^{-2}. From the intersection of the ATR scan line with the dispersion curves in figure 2, one can see that the model suggests that the ATR spectrum should have a guided mode dip, corresponding to mode 4, at 282.5 cm^{-1}; the same value could be obtained from figure 4(a) by reading off the frequency corresponding to a TO1 oscillator strength of 6170 cm^{-2}. This frequency, along with the other frequencies obtained

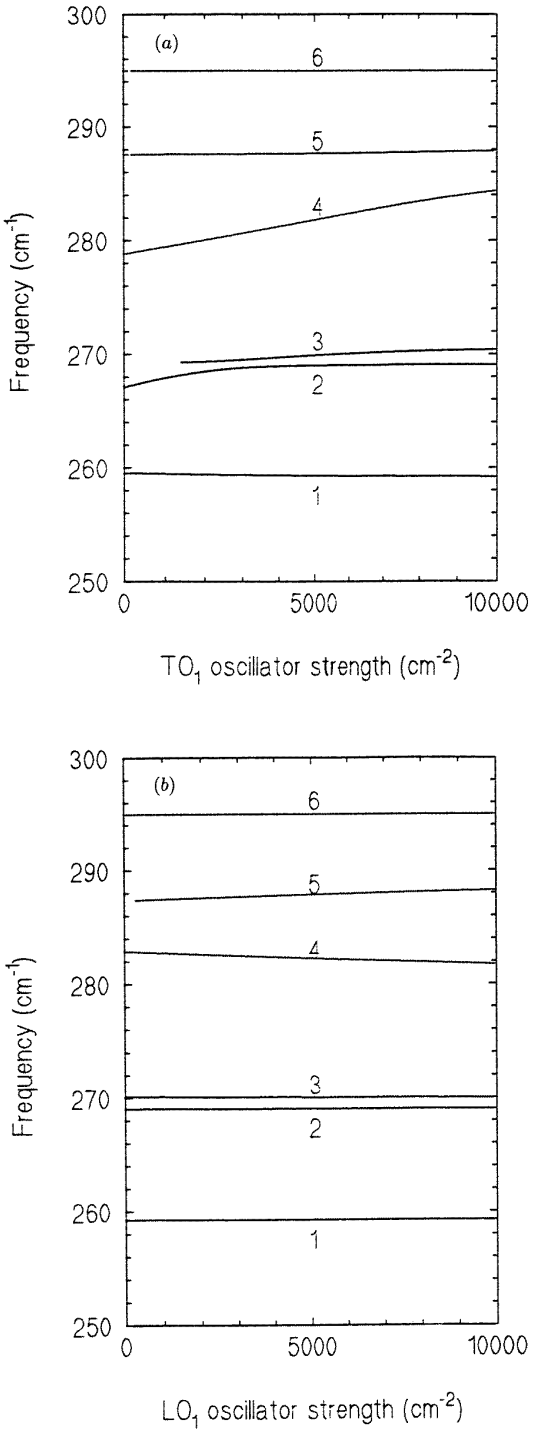

Figure 4. The effect of changing (a) the TO_1 oscillator strength and (b) the LO_1 oscillator strength on the ATR mode frequencies, assuming 20° angle of incidence from a silicon prism, determined using the same method as used to obtain the dispersion curves in figure 2.

from the dispersion curves, is marked as a vertical line in figure 1. As can be seen, the experimental frequency of the dip corresponding to mode 4 in each spectrum is somewhat lower than that anticipated from the dispersion curve. In our experiments it is therefore not sufficient to measure the position of the dip from the ATR spectra and use figure 4(a) to read off a corresponding TO_1 oscillator strength. However, it should be stressed that the positions of the dips as calculated using a full multilayer reflectivity analysis are in good agreement with the far infrared results.

The discrepancy between the experimental dips and the frequency obtained from the dispersion curve is due to the perturbing effect of the prism. This discrepancy therefore depends on the gap between the prism base and the sample. In the case of the 7 μm gap experiment, the measured dip is 1.9 cm^{-1} lower in frequency than predicted by the dispersion curve, whereas for the 12 μm gap experiment, it is only 0.7 cm^{-1} lower. It is therefore advisable to use a fairly large gap for the ATR experiment; if the gap is small it is important to have a good estimate of the size of the gap. In modelling the present experiments we simply used the thicknesses of the copper spacers used in obtaining the gap, and this indeed appears to give good agreement with theory.

The results presented here show that the TO_1 oscillator strength obtained by the linear chain model agrees well with experiment, although the other oscillator strengths are not obtained so easily. Thus it can be seen that, provided that the experiments are performed and analysed correctly, ATR spectra may be used as a sensitive measure of TO oscillator strengths in superlattices. For the superlattice system described here, p-polarization spectra proved the most useful in this respect. However, for different thicknesses of superlattice, guided wave modes in s-polarization may prove equally sensitive [15].

Appendix. Use of transfer matrix methods in determining surface and guided wave polariton dispersion curves

The use of transfer matrix methods for calculating reflectivity from multilayer structures incorporating superlattices has been detailed in, for instance, [1]. Although the superlattice is considered as a uniaxial medium in such cases, the presence of a substrate, and possible buffer or capping layers means that a multilayer analysis is still necessary, and a transfer matrix approach is normally warranted. In this appendix we adapt such a multilayer analysis for the numerical determination of dispersion curves of surface or guided wave polariton modes.

Consider p-polarized radiation in an $(N+1)$-layer system in which layer 0 (the top layer) and layer N (the bottom layer) are semi-infinite. The z-direction is normal to the layers, and in each layer n, the wavevector is of the form $(q_x, 0, q_{zn})$ where, in a uniaxial layer, q_{zn} is given by

$$q_{zn}^2 = \varepsilon_{xx,n}\frac{\omega^2}{c^2} - \frac{\varepsilon_{xx,n}}{\varepsilon_{zz,n}}q_x^2. \tag{A1}$$

Normally, of course, only one of the layers (the superlattice layer) in the structure will be uniaxial, the other layers being isotropic. However, the isotropic layers can be treated as uniaxial layers with $\varepsilon_{xx,n}$ equal to $\varepsilon_{zz,n}$.

The magnetic field component H_{yn} in each layer may be written as a sum of upward and downward rays in two alternative forms:

$$H_{yn} = a_{nl}\exp[-\mathrm{i}q_{zn}(z - z_{n,n+1})] + b_{nl}\exp[\mathrm{i}q_{zn}(z - z_{n,n+1})] \tag{A2}$$

$$H_{yn} = a_{nu}\exp[-\mathrm{i}q_{zn}(z - z_{n-1,n})] + b_{nu}\exp[\mathrm{i}q_{zn}(z - z_{n-1,n})] \tag{A3}$$

$z_{n,n+1}$ and $z_{n-1,n}$ are the positions of the interfaces at the bottom and top respectively of layer n. a_{nl} and b_{nl} represent the complex H_y fields of the downward and upward waves respectively within the layer at its lower interface, and a_{nu} and b_{nu} are the equivalent fields at its upper interface. Thus in (A2) we take the lower interface as the local origin whereas in (A3) we take the upper interface.

Rearrangement of (A2) and (A3) allows the fields at the lower and upper interfaces to be related through a transfer matrix equation

$$\begin{pmatrix} a_{nu} \\ b_{nu} \end{pmatrix} = F_n \begin{pmatrix} a_{nl} \\ b_{nl} \end{pmatrix} \tag{A4}$$

where

$$F_n = \begin{pmatrix} \exp(-\mathrm{i}q_{zn}d_n) & 0 \\ 0 & \exp(\mathrm{i}q_{zn}d_n) \end{pmatrix} \tag{A5}$$

with $d_n(= z_{n-1,n} - z_{n,n+1})$ the thickness of the layer.

In order to relate the fields at either side of each interface we use the continuity of H_y and E_x across the interface. The relationship between these fields may once again be expressed through a transfer matrix. Across the interface at $z_{n,n+1}$ the result is:

$$\begin{pmatrix} a_{nl} \\ b_{nl} \end{pmatrix} = M_{n,n+1} \begin{pmatrix} a_{(n+1)u} \\ b_{(n+1)u} \end{pmatrix} \tag{A6}$$

where

$$M_{n,n+1} = \frac{1}{2} \begin{pmatrix} 1 + \varepsilon_{xx,n}q_{z(n+1)}/\varepsilon_{xx,n+1}q_{zn} & 1 - \varepsilon_{xx,n}q_{z(n+1)}/\varepsilon_{xx,n+1}q_{zn} \\ 1 - \varepsilon_{xx,n}q_{z(n+1)}/\varepsilon_{xx,n+1}q_{zn} & 1 + \varepsilon_{xx,n}q_{z(n+1)}/\varepsilon_{xx,n+1}q_{zn} \end{pmatrix}. \tag{A7}$$

The amplitudes of the fields in the top and bottom layers can now be related by multiplying out the matrices representing field transfer across the layers and interfaces:

$$\begin{pmatrix} a_{0l} \\ b_{0l} \end{pmatrix} = M_{01} \prod_{n=1}^{N-1} F_n M_{n,n+1} \begin{pmatrix} a_{Nu} \\ b_{Nu} \end{pmatrix} = \begin{pmatrix} r_{11} & r_{12} \\ r_{21} & r_{22} \end{pmatrix} \begin{pmatrix} a_{Nu} \\ b_{Nu} \end{pmatrix}. \tag{A8}$$

In the case of a surface polariton or guided wave mode, there can be no downward ray in the top layer (layer 0) or upward ray in the bottom layer (layer N). It therefore follows that the condition for such modes to occur is

$$a_{0l} = 0 \qquad b_{Nu} = 0. \tag{A9}$$

Substitution into (A8) leads to

$$r_{11} = 0 \tag{A10}$$

(A10) can be solved by standard root finding techniques using numerical multiplication of the matrices in (A8). Thus mode frequencies may be obtained at various values of q_x to obtain dispersion curves of the type shown in figure 2.

The above analysis is for p-polarization modes. The analysis may be adapted for s-polarization modes in a straightforward manner.

References

[1] Dumelow T, Parker T J, Smith S R P and Tilley D R 1993 *Surf. Sci. Reports* **17** 151

[2] Dumelow T, Hamilton A A, Parker T J, Tilley D R, Samson B, Smith S R P, Hilton D, Moore K J and Foxon C T B 1992 *Optical Characterization of Semiconductors* ed D B Kushev (Zürich: Trans Tech) p 183

[3] Dumelow T, El-Gohary A R, Hamilton A, Maslin K A, Parker T J, Raj N, Samson B, Smith S R P, Tilley D R, Dobson P J, Foxon C T B, Hilton D and Moore K 1990 *Mater. Sci. Eng.* B **5** 205

[4] Dumelow T, Hamilton A A, Parker T J, Tilley D R, Foxon C T B, Hilton D and Moore K J 1990 *Int. J. Infrared Millimeter Waves* **11** 901
[5] Pusep Yu A, Mileken A G, Sinyukov M P, Ploog K and Toropov A I 1990 *Pis'ma Zh. Eksp. Teor. Fiz.* **52** 1068 [1991 *JETP Letters* **52** 464]
[6] Dumelow T, Hamilton A A, Parker T J, Samson B, Smith S R P, Tilley D R, Beall R B, Harris J J, Moore K J, Foxon C T B and Hilton D 1991 *Light Scattering in Semiconductor Structures and Superlattices* ed J Lockwood and J F Young (New York: Plenum) p 461
[7] Scamarcio G, Tapfer L, König W, Fischer A, Ploog K, Molinari E, Baroni S, Giannozzi P and de Gironcoli S 1991 *Phys. Rev.* B **43** 14 754
[8] Samson B, Dumelow T, Hamilton A A, Parker T J, Smith S R P, Tilley D R, Foxon C T, Hilton D and Moore K J 1992 *Phys. Rev.* B **46** 2375
[9] Pusep Yu, Milekhin A and Porokov A 1993 *Superlattices and Microstructures* **13** 115
[10] Lou B, Sudharsanan R and Perkowitz S 1988 *Phys. Rev.* B **38** 2212
[11] Dumelow T, Hamilton A A, Parker T J, Tilley D R, Beall R B, Harris J J, Hilton D, Moore K J and Foxon C T B 1992 *Optical Characterization of Semiconductors* D B Kushev (Zürich: Trans Tech) p 191
[12] El-Gohary A R, Parker T J, Raj N, Tilley D R, Dobson P J, Hilton D and Foxon C T 1989 *Semicond. Sci. Technol.* **4** 388
[13] Dumelow T, Hamilton A A, Parker T J, Samson B, Smith S R P, Tilley D R, Hilton D, Moore K J and Foxon C T B 1990 *Phonons 89* ed S Hunklinger, W Ludwig and G Weiss (Singapore: World Scientific) p 961
[14] Haraguchi M, Fukui M and Muto S 1990 *Phys. Rev.* B **41** 1254
[15] Dumelow T and Tilley D R 1993 *J. Opt. Soc. Am.* A **10** 633
[16] Samson B, Smith S R P, Foxon C T, Hilton D and Moore K J 1991 *Solid State Commun.* **78** 325
[17] Chu H and Chang Y-C 1988 *Phys. Rev.* B **38** 12 369
[18] Otto A 1968 *Z. Phys.* **216** 398
[19] Berreman D W 1963 *Phys. Rev.* **130** 2193